

In situ magnetization switching of magnetic probes applied to spin-polarized scanning tunneling microscopy

Pin-Jui Hsu,¹ Chun-I. Lu,¹ Szu-Wei Chen,¹ Wang-Jung Hsueh,¹ Yu-Hsun Chu,¹ Chuang-Han Hsu,¹ Christopher John Butler,¹ and Minn-Tsong Lin^{1,2,a)}

¹Department of Physics, National Taiwan University, 10617 Taipei, Taiwan

²Institute of Atomic and Molecular Sciences, Academia Sinica, 10617 Taipei, Taiwan

(Received 25 December 2009; accepted 11 March 2010; published online 9 April 2010)

Soft magnetic tip was utilized to be the probe of spin-polarized scanning tunneling microscopy. It was demonstrated that the spin contrast can be reversed by *in situ* switching tip magnetization through varying tip-substrate distance for resolving perpendicular magnetic domain images. With this *in situ* magnetization direction switching of the soft magnetic tip, it is conceivable to separate magnetic from chemical and topographic contributions without applying external magnetic field. This provides an effective tool for the study of complex magnetic spin structures with various nonmagnetic impurities or compositions involved. © 2010 American Institute of Physics. [doi:10.1063/1.3380711]

With the development of spin-polarized scanning tunneling microscopy (SP-STM) techniques, numerous fascinating magnetic spin structures have been unveiled and lateral resolution down to atomic scale of magnetic images can be achieved.¹⁻⁶ In the SP-STM experiments, spin-polarized probes play the crucial role and different probes were developed according to different approaches of operation modes. For example, there were optically pumped GaAs tip,⁷ magnetic materials coated W tip,^{8,9} coils wound CoFeSiB tip,¹⁰ etc., reported in previous studies. Besides, in order to have in-plane or out-of-plane spin direction identification, tips designed with different geometric shapes^{11,12} or coated with varied magnetic materials^{13,14} have been demonstrated.

However, there are still several critical issues on spin-polarized tips designed for SP-STM experiments.^{13,15} One of them is to separate the magnetic from topographic and chemical contributions with the opportunity of magnetization direction switching of either the sample or the tip. As reported by the previous SP-STM experiments,^{6,8,16,17} owing to both sample and tip were under strong external magnetic field applied, magnetization direction rotation needed to be carefully controlled to have magnetization switching of sample or tip only. Instead of applying external magnetic field, recent theoretical studies also reported that varying tip-substrate distance was capable to switch a single spin through the competition of direct and indirect exchange coupling.¹⁸⁻²⁰ In light of this, soft magnetic materials with low coercivity field for spin-polarized probe arise to be an appropriate candidate for *in situ* magnetization switching in the SP-STM technique.

In this letter, soft magnetic tip from FeMnC alloy material has been applied to be the spin-polarized probe with out-of-plane spin sensitivity for the Co nanoislands grown on Cu(111) with out-of-plane magnetization.^{16,21} Most importantly, in order to have magnetic signals distinguished, an *in situ* switching of the tip magnetization direction can be achieved through varying tip-substrate distance, revealing

the magnetic domain of Co nanoislands with reversed spin contrast.

The experiment was carried out in a UHV chamber with base pressure of $\approx 3 \times 10^{-11}$ mbar. The Cu(111) substrate was cleaned by cycles of 1 keV Ar⁺ sputtering and annealing at 850 K. After that, submonolayer Co was evaporated on the Cu(111) at room temperature through molecular beam epitaxy technique with the deposition rate of 0.6 ML min⁻¹ calibrated from STM. After sample preparation, it was subsequently transferred into low temperature STM (Omicron LT-STM) cooled at 4.4 K with pressure of $\approx 2 \times 10^{-12}$ mbar.

The tip probe of FeMnC alloy material was first prepared by mechanical milling and the corresponding magnetic properties were checked with the magneto-optic Kerr effect (MOKE) measurements. As shown in the Fig. 1(a), the small coercivity and switching field ($< 15 \pm 1$ Oe) can be characterized from the magnetic hysteresis loop. In addition, the tip image taken from scanning electron microscopy (SEM) is shown in the Fig. 1(b).

After the tip transferred into UHV chamber, it was further sputtered by 3 KeV Ar⁺ bombardment. Furthermore, in order to improve the spin contrast^{10,12} and keep coercivity to remain small available for magnetization switching, a few monolayers of Co was coated. The magnetic stability was warranted in such Co coated tip at regular tunneling distance, so that they can be applied to spin-resolved tunneling spectroscopy measurements with reliability. As for the tunneling

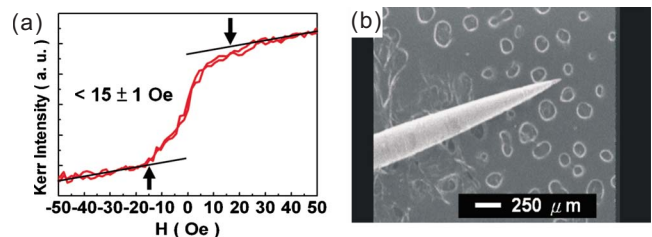


FIG. 1. (Color online) (a) Magnetic hysteresis loop of FeMnC alloy tip from the MOKE measurements and the switching field smaller than 15 ± 1 Oe can be characterized. (b) Magnified image of soft magnetic tip taken by the SEM.

^{a)}Author to whom correspondence should be addressed. Electronic mail: mtlin@phys.ntu.edu.tw.

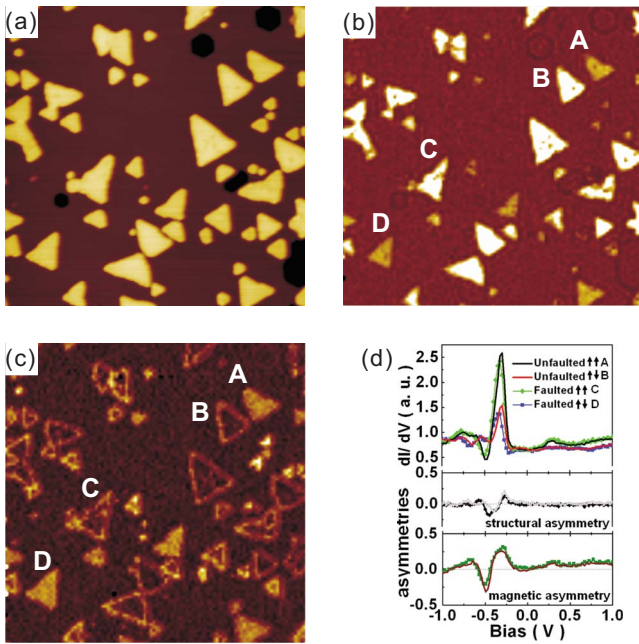


FIG. 2. (Color online) (a) Topographic image of 0.35 ML bilayer high Co nanoislands grown on Cu(111) (image size $100 \times 100 \text{ nm}^2$, $U = +1.0 \text{ V}$, and $I = 1.0 \text{ nA}$). (b) and (c) are the spin-polarized conductance mapping images recorded at -316 mV and -494 mV , respectively. (d) Top: spin-polarized conductance curves recorded from two set of Co nanoislands with same stackings and nearly same sizes as indicated from A to D in the inset of (b) and (c). Bottom: structural and magnetic asymmetry curves.

spectroscopy measurements, the feedback loop was open and the sample bias ramped from $+1.0$ to -1.0 V whereas the distance between the tip and sample was stabilized typically at scanning parameters of $+1.0 \text{ V}$ and 1.0 nA . The differential conductance spectra were recorded simultaneously to the topographic images by adding a voltage modulation of $20 \text{ mV}_{\text{rms}}$ to the sample bias and detecting the signals by the lock-in technique.

A typical STM topography of 0.35 ML Co grown on Cu(111) is shown in Fig. 2(a). There are two kinds of Co nanoisland arrangements, faulted and unfaulted fcc stackings, protruding with bilayer height from the Cu surface.^{22,23} By using the magnetic tip, the spin-polarized conductance mapping resolved at bias of -316 mV and -494 mV are presented in Figs. 2(b) and 2(c), respectively. In order to prevent the influence from crystalline and size dependent peak position of surface state,^{16,24} we discuss the conductance curves on Co nanoislands with equal stackings and sizes, as the two sets of them marked from A to D in the Figs. 2(b) and 2(c). And their corresponding conductance curves depicted with different colors are shown in top of Fig. 2(d). The prominent surface state peak of conductance curve at around -0.31 V is consistent with previous studies^{16,23} and contributes to the significant spin-polarization amplitude due to the hybridization of s - p states with the minority $d_{3z^2-r^2}$ band of Co nanoislands. The structural and magnetic asymmetry curves defined as^{13,16}

$$A_{\text{structural}} \equiv \frac{dI/dV_{\text{unfaulted}\uparrow\uparrow(\downarrow)} - dI/dV_{\text{faulted}\uparrow\uparrow(\downarrow)}}{dI/dV_{\text{unfaulted}\uparrow\uparrow(\downarrow)} + dI/dV_{\text{faulted}\uparrow\uparrow(\downarrow)}},$$

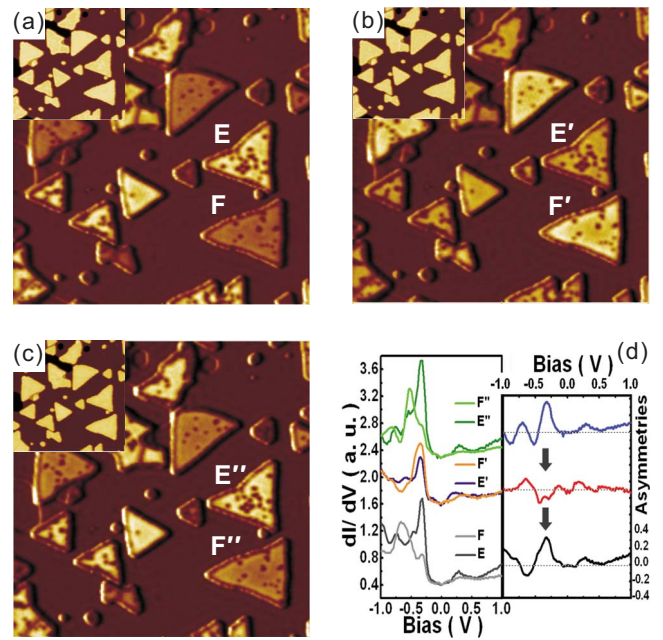


FIG. 3. (Color online) (a) Spin polarized conductance mapping image of 0.66 ML bilayer high Co nanoislands and the black spots on the surface of Co nanoislands are segregated Cu atoms. The corresponding topography is shown in the inset. (b) Reversed spin contrast image taken after the magnetization switching of front tip end. (c) Similar spin contrast image to the (a) taken after tip magnetization reverse again. (d) Tunneling spectra of a set of two Co nanoislands taken before and after magnetization switchings of tip end. (image sizes are all $85 \times 85 \text{ nm}^2$, taken at $U = -0.3 \text{ V}$ and $I = +1.0 \text{ nA}$).

$$A_{\text{magnetic}} \equiv \frac{dI/dV_{(\text{un})\text{faulted}\uparrow\downarrow} - dI/dV_{(\text{un})\text{faulted}\downarrow\downarrow}}{dI/dV_{(\text{un})\text{faulted}\uparrow\downarrow} + dI/dV_{(\text{un})\text{faulted}\downarrow\downarrow}},$$

are shown in the bottom of Fig. 2(d). The conductance curves from these two different derivations can thus be clearly distinguished. Besides, the characteristic oscillatory behavior of magnetic asymmetry due to the sign reversal of spin polarization is also observed, being consistent with previous studies.¹⁶

After the magnetic domain images and spin-polarized conductance spectra have been resolved, the reversal spin contrast recorded at bias of -0.3 V and 1.0 nA are sequentially demonstrated in Figs. 3(a)–3(c). At first, the topography of 0.66 ML Co nanoislands and the spin-polarized conductance mapping, recorded simultaneously, are shown in the inset of Fig. 3(a) and Fig. 3(a), respectively. The spin contrast of these nanoislands can be clearly observed according to the magnetization direction parallel or antiparallel to that of the magnetic tip.²⁵ Besides the spin contrast, some black spots on the surface of Co nanoislands are also observed due to the segregation of Cu atoms.²⁶ Afterward we move the tip to one of Co nanoislands, as shown by F in Fig. 3(a), with the magnetization antiparallel to the tip magnetization, and decrease the tip-substrate distance by reducing the bias to 3 mV and increasing the current to 30 nA , which is much smaller than the current used in the spin injection of previous SP-STM experiments.²⁷ The corresponding conductance is $\sim 0.258G_0$, where $G_0 \equiv e^2/h$ is for two magnetic electrodes without spin degeneracy.^{28,29} After that, we go back to the normal scanning parameters of -0.3 V and 1.0 nA , and the reversal spin contrast of all Co islands can be clearly observed in the Fig. 3(b). By repeating this

process at another Co nanoisland E' of Fig. 3(b), we can reverse again the spin contrast images as shown in the Fig. 3(c) similar to the Fig. 3(a). This demonstrates the magnetization direction of tip end can conceivably be reversed back by such kind of operation. In addition, for the segregated Cu atoms, i.e., black spots on the surface of Co nanoislands in the spin contrast images, there is no contrast between them during the magnetization switchings of tip end. Separation of magnetic signal from topographic or chemical contributions could be thus achieved in such way.

The tunneling spectroscopy measurements before and after tip magnetization switchings are also presented in the Fig. 3(d). From the comparison of spin-polarized conductance curves of E and F taken from Co nanoislands indicated in the Fig. 3(a), curve E has stronger amplitude than curve F at around -0.3 V and curve F has stronger amplitude than curve E at around -0.5 V on the contrary.¹⁶ Such behavior reverses in the curves of E' and F' due to the magnetization switching of front tip end and reverses back again in the curves of E'' and F'' . Besides, from the asymmetry curves illustrated in the Fig. 3(d), the major contribution to reversal spin contrast image can be indicated by the arrows in the bias voltage region of spin-polarized surface state. The slight difference in the asymmetry curves, especially at around -0.7 V (Ref. 16) which is not reversed accordingly, might come from the complex intra-atomic noncollinear magnetism of the magnetic tip end³⁰ and requires further studies in the future. Nevertheless, the tip magnetization switching behavior is much more clear and can be identified from the pronounced spin-polarized surface state at around -0.3 V.

In summary, FeMnC alloy materials with low coercivity field have been applied to be the spin-polarized probe with the capability of *in situ* magnetization direction switching. According to the consequential reversal spin contrast of Co nanoislands, tip magnetization switching can be achieved through reducing tip-substrate distance. This provides an effective method to distinguish magnetic signals from chemical or topographic contributions without applying external magnetic field in the SP-STM.

We acknowledge financial support from the National Science Council of Taiwan under Grant No. NSC 98-2120-M-002-010.

¹R. Wiesendanger, I. V. Shvets, D. Bürgler, G. Tarrach, H. J. Güntherodt, J. M. D. Coey, and S. Gräser, *Science* **255**, 583 (1992).

- ²S. Heinze, M. Bode, A. Kubetzka, O. Pietzsch, X. Nie, S. Blügel, and R. Wiesendanger, *Science* **288**, 1805 (2000).
- ³H. Yang, A. R. Smith, M. Prikhodko, and W. R. L. Lambrecht, *Phys. Rev. Lett.* **89**, 226101 (2002).
- ⁴N. Berdunov, S. Murphy, G. Mariotto, and I. Shvets, *Phys. Rev. Lett.* **93**, 057201 (2004).
- ⁵C. L. Gao, U. Schlickum, W. Wulfhchel, and J. Kirschner, *Phys. Rev. Lett.* **98**, 107203 (2007).
- ⁶M. Bode, M. Heide, K. von Bergmann, P. Ferriani, S. Heinze, G. Bihlmayer, A. Kubetzka, O. Pietzsch, S. Blügel, and R. Wiesendanger, *Nature (London)* **447**, 190 (2007).
- ⁷S. F. Alvarado and P. Renaud, *Phys. Rev. Lett.* **68**, 1387 (1992).
- ⁸A. Kubetzka, M. Bode, O. Pietzsch, and R. Wiesendanger, *Phys. Rev. Lett.* **88**, 057201 (2002).
- ⁹T. K. Yamada, M. M. J. Bischoff, T. Mizoguchi, and H. van Kempen, *Appl. Phys. Lett.* **82**, 1437 (2003).
- ¹⁰H. F. Ding, W. Wulfhchel, and J. Kirschner, *Europhys. Lett.* **57**, 100 (2002).
- ¹¹C. B. Wu, P. J. Hsu, H. Y. Yen, and M.-T. Lin, *Appl. Phys. Lett.* **91**, 202507 (2007).
- ¹²U. Schlickum, W. Wulfhchel, and J. Kirschner, *Appl. Phys. Lett.* **83**, 2016 (2003).
- ¹³M. Bode, *Rep. Prog. Phys.* **66**, 523 (2003).
- ¹⁴J. Prokop, A. Kukunin, and H. J. Elmers, *Phys. Rev. B* **73**, 014428 (2006).
- ¹⁵R. Wiesendanger, *Rev. Mod. Phys.* **81**, 1495 (2009).
- ¹⁶O. Pietzsch, A. Kubetzka, M. Bode, and R. Wiesendanger, *Phys. Rev. Lett.* **92**, 057202 (2004).
- ¹⁷O. Pietzsch, A. Kubetzka, M. Bode, and R. Wiesendanger, *Science* **292**, 2053 (2001).
- ¹⁸R. Z. Huang, V. S. Stepanyuk, A. L. Klavysyuk, W. Hergert, P. Bruno, and J. Kirschner, *Phys. Rev. B* **73**, 153404 (2006).
- ¹⁹K. Tao, V. S. Stepanyuk, P. Bruno, D. I. Bazhanov, V. V. Maslyuk, M. Brandbyge, and I. Mertig, *Phys. Rev. B* **78**, 014426 (2008).
- ²⁰K. Tao, V. S. Stepanyuk, W. Hergert, I. Rungger, S. Sanvito, and P. Bruno, *Phys. Rev. Lett.* **103**, 057202 (2009).
- ²¹O. Pietzsch, S. Okatov, A. Kubetzka, M. Bode, S. Heinze, A. Lichtenstein, and R. Wiesendanger, *Phys. Rev. Lett.* **96**, 237203 (2006).
- ²²N. N. Negulyaev, V. S. Stepanyuk, P. Bruno, L. Diekhoner, P. Wahl, and K. Kern, *Phys. Rev. B* **77**, 125437 (2008).
- ²³L. Diekhöner, M. A. Schneider, A. N. Baranov, V. S. Stepanyuk, P. Bruno, and K. Kern, *Phys. Rev. Lett.* **90**, 236801 (2003).
- ²⁴M. V. Rastei, B. Heinrich, L. Limot, P. A. Ignatiev, V. S. Stepanyuk, P. Bruno, and J. P. Bucher, *Phys. Rev. Lett.* **99**, 246102 (2007).
- ²⁵M. Julliere, *Phys. Lett. A* **54**, 225 (1975).
- ²⁶A. Rabe, N. Memmel, A. Steltempohl, and Th. Fauster, *Phys. Rev. Lett.* **73**, 2728 (1994).
- ²⁷S. Krause, L. Berbil-Bautista, G. Herzog, M. Bode, and R. Wiesendanger, *Science* **317**, 1537 (2007).
- ²⁸N. Néel, J. Kröger, and R. Berndt, *Phys. Rev. Lett.* **102**, 086805 (2009).
- ²⁹V. Rodrigues, J. Bettini, P. C. Silva, and D. Ugarte, *Phys. Rev. Lett.* **91**, 096801 (2003).
- ³⁰M. Bode, O. Pietzsch, A. Kubetzka, S. Heinze, and R. Wiesendanger, *Phys. Rev. Lett.* **86**, 2142 (2001).